

# The rotational spectra of the $\nu_8 = \nu_9 = 1$ and $\nu_6 = \nu_7 = 1$ interacting vibrational states of nitric acid ( $\text{HNO}_3$ )

Douglas T. Petkie<sup>a,\*</sup>, Paul Helminger<sup>b</sup>, Ivan R. Medvedev<sup>c</sup>, Frank C. De Lucia<sup>c</sup>

<sup>a</sup> Departments of Physics and Electrical Engineering, Wright State University, Dayton, OH 45435, USA

<sup>b</sup> Department of Physics, University of South Alabama, Mobile, AL 36688, USA

<sup>c</sup> Department of Physics, Ohio State University, Columbus, OH 43210, USA

## ARTICLE INFO

### Article history:

Received 11 March 2010

In revised form 25 March 2010

Available online 9 April 2010

### Keywords:

Nitric acid

Rotational spectroscopy

Torsional splitting

Fermi resonance

Combination states

## ABSTRACT

The analysis of the rotational spectrum of  $\text{HNO}_3$  has been extended to include the  $\nu_8 = \nu_9 = 1$  state at  $1205.7 \text{ cm}^{-1}$  and the  $\nu_6 = \nu_7 = 1$  state at  $1223.4 \text{ cm}^{-1}$ . Based on 78–519 GHz data, the assignments in the  $8^19^1$  vibrational state have been significantly expanded from the previously reported microwave measurements [T.M. Goyette, F.C. De Lucia, *J. Mol. Spectrosc.* 139 (1990) 241–243]. A new microwave analysis is also reported for the  $6^17^1$  vibrational state. A simultaneous analysis takes into account the localized  $\Delta K_a = \pm 2$  Fermi resonances between the vibrational states, describes the torsional splitting of 3.3 and 1.4 MHz for the  $8^19^1$  and  $6^17^1$  states respectively, and fits to experimental accuracy over 1500 rotational transition frequencies that extend up to  $J = 59$ . Infrared energy levels [A. Perrin, J.-M. Flaud, F. Keller, A. Goldman, R. D. Blatherwick, F. J. Murcray, C. P. Rinsland, *J. Mol. Spectrosc.* 194 (1999) 113–123] were also included in the analysis and fit to experimental accuracy. Measurement of strongly perturbed transitions in each vibrational state provide a determination of the band origin difference of  $17.733184(17) \text{ cm}^{-1}$ . The rotational constants agree well with those predicted by vibrational–rotational constants of the fundamental modes. Furthermore, the analysis will provide a very accurate simulation of the infrared spectrum of  $\text{HNO}_3$  in the  $8.3 \mu\text{m}$  region.

© 2010 Elsevier Inc. All rights reserved.

## 1. Introduction

The millimeter (mm) wave/submillimeter (submm) wave and infrared spectrum of nitric acid continues to receive considerable attention due to its important role in the atmospheric chemistry associated with ozone destruction [1] and the increasing number of remote sensing missions capable of spectral measurements in both the mm/submm and infrared regions (see [1,2] and references therein). As an example, the MIPAS limb-sounding instrument has measured the isotopic partitioning between stratospheric  $\text{H}^{15}\text{NO}_3$  and  $\text{H}^{14}\text{NO}_3$  to have a ratio on the order of 0.00365 [3,4]. To support these missions, and for fundamental spectroscopic interest, several recent infrared studies focused on modeling the line positions, line intensities and integrated band intensities of both fundamental and hot bands. Gomez et al. [5] examined the 600–950  $\text{cm}^{-1}$  region that is dominated by the strong  $\nu_5$  and  $2\nu_9$  bands, where the latter borrows a significant intensity from the former through a strong zero-order Fermi resonance that mixes the two states [6,7]. That study focused on modeling the weaker hot bands

and incorporated more accurate pressure broadening parameters and line-mixing effects into the Q-branch hot bands to reduce the disagreements between spectral database simulations and the measured MIPAS satellite data. In other recent work, Laraia et al. [2] performed theoretical calculations for the pressure broadening half-widths of the individual lines that comprise the  $\nu_5$  infrared band to improve the database content. In most cases, hot bands are difficult to directly measure in the infrared due to limited resolution and the overlapping fundamental band as is the case in the above studies [5]. However, the rotational structure of the bands can be accurately determined by the measurement and analysis of the spectrally resolved pure rotational transitions in the microwave, mm/submm-wave region, as was demonstrated for the  $22 \mu\text{m}$  region of  $\text{HNO}_3$ , where the fundamental  $\nu_9$  band and the  $\nu_5 - \nu_9$  and  $2\nu_9 - \nu_9$  hot bands were accurately simulated [8]. All of these efforts illustrate the high level of laboratory measurements and stringent models required to achieve more accurate retrievals of the volume mixing ratio profiles of  $\text{HNO}_3$  in the atmosphere.

The weak  $\nu_8 + \nu_9$  combination band located at  $1205 \text{ cm}^{-1}$  ( $8.3 \mu\text{m}$ ) is also of high interest [9,10]. The first high-resolution analysis of the infrared spectrum was reported by Maki [11] and was followed shortly by a mm/submm-wave study by Goyette et al. [12]. In the latter case, the assignment of 107 rotational frequencies were made by utilizing Maki's predictions, the triplet structure associated

\* Corresponding author. Address: Department of Physics, 248 Fawcett Hall, Wright State University, 3640 Colonel Glenn Hwy, Dayton, OH 45435, USA. Fax: +1 (937) 775 2222.

E-mail address: [doug.petkie@wright.edu](mailto:doug.petkie@wright.edu) (D.T. Petkie).

with the torsional  $\nu_9$  mode [13,14] and a consideration of the relative intensities of the candidate lines when compared to ground state transitions. Transitions up to  $J = 38$  (15 transitions from  $J = 30$ –38) were assigned and these included several with asymmetry splitting contributions. These assignments were made without the detailed knowledge of the spectra of several stronger states ( $\nu_5 = 1$ ,  $\nu_9 = 2$ ,  $\nu_6 = \nu_9 = 1$ ,  $\nu_7 = \nu_9 = 1$ ,  $\nu_7 = 2$ , and the ground state of  $\text{H}^{15}\text{NO}_3$ ) that are now all thoroughly characterized [15–17]. In addition to this, the FASSST spectrometer used in the present study covers larger continuous spectral regions (>100 GHz) while the previous system in Ref. [12] covered much shorter continuous spans ( $\sim 100$  MHz) with more spectral congestion due to harmonic content associated with frequency-multiplier based spectrometers.

Two additional high-resolution infrared studies extended the analysis of the  $\nu_8 + \nu_9$  infrared band to incorporate the  $\Delta K_a = \pm 2$  Fermi resonance with the  $\nu_6 + \nu_7$  band that is  $\sim 20$   $\text{cm}^{-1}$  higher. Wang et al. [18] measured an extensive set of A-type infrared transitions up to  $J = 57$  and fit those, along with the previously reported mm/submm-wave data [12], in a model that required a  $\Delta K_a = \pm 2$  Fermi resonance with the  $6^17^1$  state in order to satisfactorily reproduce the observed transitions. In that fit, the  $6^17^1$  band origin and  $B$  rotational constant were free variables. Even though no  $\nu_6 + \nu_7$  infrared transitions were observed, several  $\nu_8 + \nu_9$  transitions were weaker than expected, which implied an intensity borrowing. As expected, the only perturbation clearly identified between these two states was the  $\Delta K_a = \pm 2$  Fermi resonance since the coupling between two combination states typically has a small zero-order Fermi resonance coupling term. There was no evidence of Coriolis resonances. Perrin et al. [19] performed a more extended infrared analysis that involved significantly higher quantum numbers up to  $J = 74$  along with the measurement of the weaker B-type transitions. Due to the strong local Fermi resonance, the  $J = 30$ ,  $K_a = 7$ , 8,  $K_c = 23$  rotational energy level from the  $6^17^1$  state was determined from the measurement of two  $\nu_6 + \nu_7$  transitions that borrowed intensity from corresponding  $\nu_8 + \nu_9$  transitions. The Hamiltonian in Ref. [19] was similar to that in Ref. [18] in that only one additional distortional constant for the  $8^19^1$  state and one additional  $\Delta K_a = \pm 2$  Fermi resonance term were needed as free parameters. However, the  $6^17^1$  state required eight fitted parameters (band origin, three rotational constants and four distortional parameters,  $\Delta K$ ,  $\Delta J$ ,  $\delta_J$ ,  $H_K$ ) compared to the two fitted parameters in Ref. [18], indicating the significance of the perturbation on the measured data set. Constrained parameters in each state were fixed to those used for the ground state. While a majority of the measured pure rotational transitions from Ref. [12] agreed with the predictions from the infrared analysis, 14 transitions had significant discrepancies (20+ MHz). Therefore the final infrared analysis did not include the pure rotational transitions and a table of the previously measured rotational transitions was provided along with the predicted transitions frequencies that were based on the infrared analysis. In addition to line position measurements and energy level calculations, a set of individual A- and B-type line intensities were measured to determine the transition moment operator that enabled the synthetic spectrum of the 8.3  $\mu\text{m}$  region to be generated along with a calculation of the total band intensity. This analysis allowed the transferred intensity from the 'bright'  $\nu_8 + \nu_9$  to the 'dark'  $\nu_6 + \nu_7$  infrared bands due to the local Fermi resonances to be predicted with the result that the  $\nu_6 + \nu_7$  band accounts for only  $\sim 0.2\%$  of the total integrated intensity. The additional work by Chackerian et al. [20] determined the integrated absorption cross sections over several regions from 820–5300  $\text{cm}^{-1}$  and included the  $\nu_8 + \nu_9$  combination band near 1205  $\text{cm}^{-1}$  (8.3  $\mu\text{m}$ ).

In this paper, we report the significant extension of the analysis of the  $8^19^1$  and  $6^17^1$  states in the mm/submm-wave region that includes the measurement and fitting of the torsional splitting for each state, including the  $6^17^1$  infrared dark state. This analysis pro-

vides the spectroscopic details of the torsional splitting and anharmonic resonances and a basis for a more accurate simulation of the infrared spectrum.

## 2. Experimental

The experimental techniques used to record the millimeter and submillimeter-wave spectral data reported here have been previously discussed [21–23] and will only be briefly described here. The spectra were assigned from a nearly continuous region that spans from 78 to 519 GHz with 85% coverage. From 78 to 118 GHz, and in selected regions from 118–178 GHz, computer controlled, phase-locked, BWO-based Quartz synthesizers were used for sources along with  $2f$  lock-in detection techniques. The regions above 118 GHz were recorded with the Ohio State University Fast Scan Submillimeter Spectroscopic Technique (FASSST) system, which is based on free-running BWOs with a Fabry–Perot cavity used for optical frequency calibration. The electronic detection (fast sweep and bandpass filtering) and software processing (convolution of a first derivative lineshape) result in a second derivative lineshape for measured spectral lines. Room temperature diode detectors were used below 118 GHz and liquid helium cooled InSb hot electron bolometers were used above 118 GHz. The radiation was coupled from the sources and to the detectors with lenses and propagated down a  $\sim 5$  m long, 10 cm diameter absorption cell. The nitric acid gas was drawn from a commercially available, concentrated nitric acid liquid sample mixed with sulfuric acid that was a drying agent that limited the partial pressure of water vapor. All measurements were made at pressures of approximately 10 mTorr and a slow flow of the sample gas was established due to the decomposition of nitric acid over time. In many regions, both heated ( $\sim 200$  °C) and room temperature spectra were recorded to help differentiate the pure rotational spectra of various thermally populated vibrational states during the assignment and analysis of the spectrum. The estimated accuracy of the measured transitions is 100 kHz.

## 3. Spectral analysis and results

Nitric acid has dipole moments of  $\mu_a = 1.986D$  and  $\mu_b = 0.882D$  [24] and a mm/submm-wave spectrum that is characterized by strong R-type bandheads spaced by approximately 12.5 GHz throughout the spectrum, along with weaker Q-branch transitions, as shown in Fig. 1. The assignment and analysis for the  $8^19^1$  state started with the extension of the mm/submm-wave transitions reported previously in Ref. [12]. The initial identification and assignment of specific transitions for the  $6^17^1$  state were made based on the predicted frequency shifts from the identical ground state transitions. These shifts were calculated by summing the observed frequency shifts for the identical rotational transitions in the  $6^1$  and  $7^1$  states from the ground state based on the measurements or analyses in Refs. [16,25]. Candidates were then selected based on the intensity of the transition relative to other known transitions. For many vibrational states, the torsional motion associated with the  $\nu_9$  mode splits what would be quadruply degenerate transitions in the symmetric-top limit to create a triplet structure [13,14]. The weaker b-types are split around the degenerate a-types by  $\sim 3.3$  MHz for  $8^19^1$  and  $\sim 1.4$  MHz for  $6^17^1$ , as illustrated in Fig. 2. This torsional splitting was quickly identified for the  $6^17^1$  state and it also aided the assignment process.

In the early stages of this work, the transitions for each vibrational state were fitted in separate analyses to Watson-like internal axis system (IAS) Hamiltonians (A-reduced in the  $I'$  representation) with torsional splitting parameters using the SPFIT/SPCAT program suite [26–28], similar to the analyses for the  $9^1$  state in Ref. [16] and  $7^19^1$  and  $6^19^1$  states in Ref. [15]. Once a sufficient number of

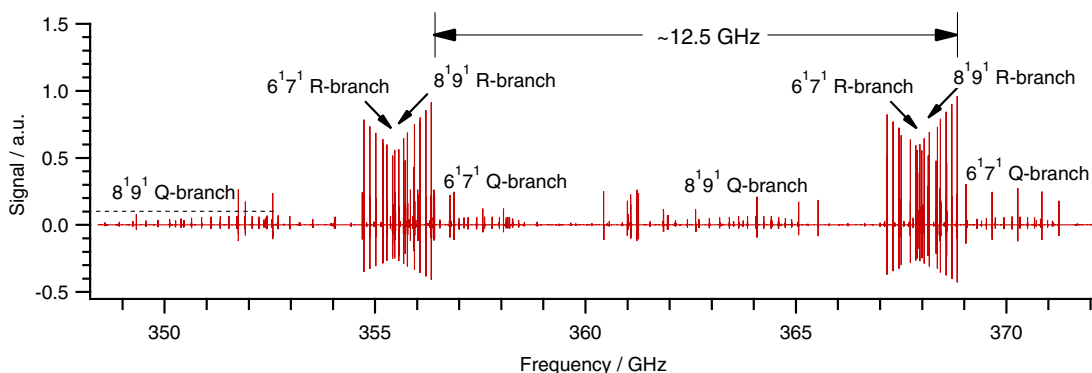


**Fig. 1.** Simulated second derivative rotational spectrum for the  $6^1 7^1$  and  $8^1 9^1$  states centered near 360 GHz over a 25 GHz span that highlights the main features of the nitric acid spectrum. The strongest spectral lines are R-branch transitions while the Q-branch lines are approximately an order of magnitude weaker as indicated by the dashed line for the  $8^1 9^1$  Q-branch spanning  $\sim 348$ – $353$  GHz.

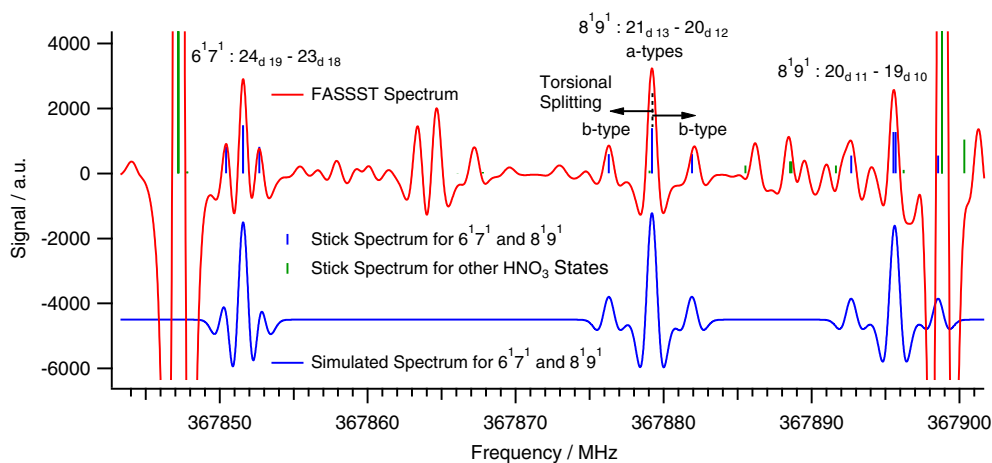


**Fig. 2.** The measured FASSST spectrum centered near 367.87 GHz (upper plot) showing triplets for each state that demonstrates the torsional splitting. The splitting of the b-type satellites from the a-type is  $\sim 3.3$  MHz for  $8^1 9^1$  and  $\sim 1.4$  MHz for  $6^1 7^1$ . The strong transition on the left is a ground state line while the one on the right is a  $\nu_7 = 1$  line. For reference, the stick spectra are also shown in the measured spectrum. The 'd' symbol represents the degenerate  $K_a$  rotational quantum number for each set of transitions.

transitions for each state were assigned, a simultaneous analysis was established that included a separate set of rotational and torsional constants for each state as well as Fermi interactions terms to account for the localized  $\Delta K_a = \pm 2$  resonances [18,19]. A Fourier series expansion of individual elements of the Hamiltonian ( $E_\rho$ ,  $E_{\rho\beta}$ ,  $E_{\rho\pm}$ ) were included to model the torsional effects. The spectroscopic constants for the final simultaneous analysis are provided in Table 1, a statistical description of the fit is given in Table 2, and the graphical coverage of the spectral data included for each state is shown in Figs. 3 and 4. For the mm/submm-wave spectral data set, the quantum state distribution and frequency coverage is similar for each vibrational state with over 1500 transitions measured in the combined analysis that include strongly perturbed transitions as indicated in Fig. 5. The infrared energy levels determined from combination differences by Perrin et al. [19,29] were included in a final microwave/infrared combined analysis. While the infrared energy level set is extensive for the  $\nu_8 + \nu_9$  mode, the  $\nu_6 + \nu_7$  mode is a 'dark' band and only one energy level was determined from the infrared spectrum. The overall rms deviation for the mm/submm-wave fit is 99 kHz for 1546 transition frequencies. The overall rms deviation for the infrared energy level data set is  $0.00042 \text{ cm}^{-1}$ , slightly better than  $0.00048 \text{ cm}^{-1}$  that was reported in Ref. [19]. However, three highly perturbed  $8^1 9^1$  energy levels at the edge of the infrared data set ( $44_{20\ 24}$ ,  $45_{20\ 25}$ ,  $45_{21\ 24}$ ) could not be satisfactorily fit in the analysis reported here, were excluded from the final fit, and are considered incorrectly assigned levels.

The base torsional splitting (i.e. at low quantum numbers) is defined here as the distance the b-type satellites are shifted (split) from the a-type transitions and is given by  $2E_\rho$ . Examples of the splitting for each state are shown in Fig. 2 and Table 3 provides a list of the torsional splittings for each nitric acid vibrational state observed to date. The splittings reported in this table are either based on fitted torsional parameter ( $2E_\rho$ ) or are estimated from the observed spectra, as is in the case of  $\nu_3 = 1$ ,  $\nu_4 = 1$ ,  $\nu_6 = 2$  and  $\nu_7 = \nu_8 = 1$ , where the last two states are tentative vibrational state assignments. Torsional splittings for the fundamental vibrational states  $\nu_7 = 1$ ,  $\nu_6 = 1$ ,  $\nu_8 = 1$  and  $\nu_2 = 1$  have not been resolved nor have the splittings for the  $\nu_7 = 2$  state. The torsional splitting, as determined for the analysis presented in Table 1, is 3.3 MHz for the  $8^1 9^1$  state and 1.4 MHz for the  $6^1 7^1$  state.

The torsional splitting for the  $6^1 7^1$  state is perhaps surprisingly large since it could be expected to be unresolved, as it is for the  $7^2$  state. Given the anharmonic resonance between the  $6^1 7^1$  and  $8^1 9^1$  states, we considered that this splitting might be 'borrowed' from the  $8^1 9^1$  as was the case for the strongly mixed  $5^1/9^2$  dyad [6,7]. In that case, the 35.4 MHz splitting in the  $5^1$  state and the 50.8 MHz splitting in the  $9^2$  state were accounted for in a Hamiltonian model that included a zero-order Fermi resonance interaction term that mixes the two states. The fitted torsional splitting parameter ( $2E_\rho$ ) for the  $9^2$  state was 86.3 MHz while the  $5^1$  state torsional parameters were fixed at zero. This model mixes the wavefunctions to accurately describe the ratio of the torsional splitting

**Table 1**  
Spectroscopic constants of HNO<sub>3</sub> in the 6<sup>1</sup>7<sup>1</sup> and 8<sup>1</sup>9<sup>1</sup> states<sup>a</sup> (in units of MHz unless noted).

Parameter	$\nu_8 = \nu_9 = 1$	$\nu_6 = \nu_7 = 1$
$\nu_0$ (cm <sup>-1</sup> )	1205.707325(11)	1223.440509(13)
$A$	12959.343(172)	12972.444(182)
$B$	11980.015(172)	12103.050(182)
$C$	6254.93685(37)	6224.74490(48)
$D_{ab}$	-185.23(46)	-217.81(36)
$D_{abK} \times 10^3$	-	-0.873(107)
$\Delta_J \times 10^3$	9.53879(58)	9.8345(42)
$\Delta_{JK} \times 10^3$	-3.9522(72)	-6.111(118)
$\Delta_K \times 10^3$	5.1908(102)	7.610(176)
$\delta_J \times 10^3$	4.179053(278)	4.01988(215)
$\delta_K \times 10^3$	7.46907(269)	8.762(52)
$\Phi_J \times 10^9$	40.328(188)	9.66(53)
$\Phi_{JK} \times 10^7$	-1.5615(308)	-0.943(50)
$\Phi_{KJ} \times 10^7$	2.095(98)	1.307(65)
$\Phi_K \times 10^8$	-7.59(72)	-
$\varphi_J \times 10^8$	3.0133(94)	-1.1259(259)
$\varphi_{JK} \times 10^9$	3.19(170)	-16.83(209)
$\varphi_K \times 10^7$	1.1250(266)	1.5668(155)
$l_{KJ} \times 10^{12}$	-3.295(223)	-
$l_K \times 10^{12}$	-3.46(57)	-
<i>Fourier expansion of rotational constants</i>		
$\rho$ (dimensionless) <sup>b</sup>	1.469105	1.467300
$E_\rho$	-1.6441(55)	-0.7208(51)
$E_{\rho J} \times 10^3$	-0.7469(62)	-0.1040(78)
$E_{\rho \pm} \times 10^3$	0.4089(45)	-
<i>Interaction constants</i>		
$F_\pm$		5.23270(67)
$F_{\pm J} \times 10^3$		-0.42173(65)
$F_{\pm K} \times 10^3$		0.28812(219)
$F_{\pm JK} \times 10^8$		1.318(95)
<i>Fourier expansion of interaction constants</i>		
$F_{\rho \pm} \times 10^4$		-9.89(49)

<sup>a</sup> Estimated errors in parenthesis represent one standard deviation.

<sup>b</sup> The ratio of the moment of inertia of the top to that of the frame,  $\rho$ , cannot be fit for in SPFIT and was empirically adjusted to minimize the rms deviation of the fit.

**Table 2**  
Statistical analysis of data and fit.

	$\nu_8 = \nu_9 = 1$	$\nu_6 = \nu_7 = 1$
<i>Microwave data</i>		
Number of transitions	903	643
$J_{max}, K_a, K_c, K_c, max$	59, 39, 41	58, 35, 41
$\sigma_{fit}$ (MHz)	0.101	0.099
<i>Infrared data<sup>a</sup></i>		
Number of energy levels	1792	1
$J_{max}, K_a, K_c, K_c, max$	74, 49, 74	30, 7, 23
$\sigma_{fit}$	$0.42 \times 10^{-3} \text{cm}^{-1}$	

<sup>a</sup> From Perrin et al. [19,29].

between the two states as well as the ratio of the infrared band intensities. If a strong zero-order Fermi resonance were to explain the 6<sup>1</sup>7<sup>1</sup> state torsional splitting, then one would expect the infrared bands to have the intensity ratio that followed the ratio of the torsional splittings. Specifically, the  $\nu_6 + \nu_7$  band should be 0.40 the intensity of the  $\nu_8 + \nu_9$  band. However, the  $\nu_6 + \nu_7$  infrared band has not been reported to be present at that intensity [10] and the only reported intensity borrowing in the high-resolution analyses in Refs. [18,19] is associated with the localized Fermi resonances shown in Figs. 3 and 4 for isolated levels with only two  $\nu_6 + \nu_7$  transitions measured in Ref. [19]. Consequently, we have used a separate set of torsional parameters for each state and expect that the torsional splitting in the 6<sup>1</sup>7<sup>1</sup> vibrational state is due to a weak anharmonic resonance with a state that has a large torsional splitting, such as the  $\nu_9 = 4$  state whose torsional levels are split by

~27 GHz [30]. This was the case for the unexpectedly large torsional splitting in the 7<sup>1</sup>9<sup>1</sup> and 6<sup>1</sup>9<sup>1</sup> states in Ref. [15] that have a weak anharmonic resonance with the  $\nu_9 = 3$  state whose torsional levels are split by ~1.7 GHz [30]. In addition to this, if a vibrational wavefunction mixing due to a zero-order Fermi resonance were present, one would also expect the rotational constants to be averaged between the mixed states as was the case for chlorine nitrate when the zero-order Fermi resonance was constrained to zero [31,32]. In contrast, we show the absence of any such averaging in the discussion that follows.

To compare the rotational constants for the vibrational states reported here to those of the fundamental modes reported previously [16], the constants must be rotated from the internal axis system to the principal axis system [15]. These constants can then be compared to the ground state rotational constants to determine the vibrational-rotational constants,  $\Delta R_\nu = \alpha_\nu^R = R_{gs} - R_\nu$ , for each vibrational state  $\nu$  where  $R = A, B, C$  are the rotational constants. Table 4 shows that the vibrational-rotational constants are well predicted from the fundamental vibrational states reported in Ref. [16] and are also well predicted by *ab initio* calculations of Gutle et al. [33] using the B3LYP/6-311+G(3df,2pd) level calculation. This supports the assumption that the zero-order Fermi interaction is negligible as the rotational constants are not averaged together. Table 4 also provides the fitted rotational constants from Refs. [18,19] that were used to satisfactorily reproduce the observed infrared spectrum in the  $\nu_8 + \nu_9$  band. In such infrared analyses, it is common to fix any undeterminable constants of a 'dark' state to those values reported for the ground state and free up any constants required to fit the data in the 'bright' state. However, it may be advantageous and more physical to constrain any fitted rotational constants of an infrared dark state to those determined by microwave analysis or by *ab initio* predictions when either of these is available. Otherwise, the lack of spectral data and the correlations with other constants, particularly due to the Fermi resonance terms, could lead to unnecessarily large discrepancies. While Table 4 shows that the  $B$  rotational constant for the 6<sup>1</sup>7<sup>1</sup> state was well determined in a simultaneous fit of the bright and dark infrared bands in Refs. [18,19], the  $A$  and  $C$  rotational constants, as well as several distortional constants in Ref. [19], are not in good agreement, as will be discussed in further detail below.

The extensive rotational data set for each vibrational state along with the measurement of strongly perturbed transitions provided a determination of the band origin difference between the 8<sup>1</sup>9<sup>1</sup> and 6<sup>1</sup>7<sup>1</sup> states to be 17.733184(17) cm<sup>-1</sup>. This can be compared to the differences found in Ref. [18] of 17.1415(38) cm<sup>-1</sup> and Ref. [19] of 16.972(34) cm<sup>-1</sup>. The large discrepancy in comparison to the uncertainties of the previous reported values has several reasons. The main reason is the 6<sup>1</sup>7<sup>1</sup> state's energy levels in the infrared analyses were primarily determined via their effect on the 8<sup>1</sup>9<sup>1</sup> state as the  $\nu_6 + \nu_7$  band is dark and could not be measured directly, with the exception of two infrared transitions in Ref. [19]. In addition to this, for the analysis in Ref. [19], the strong localized resonances at higher quantum numbers (primarily  $J > 30$ ), the three incorrectly assigned energy levels at the edge of the infrared data set near  $J = 44, K_c = 25$  identified above, and the need for a large number of free parameters in the 6<sup>1</sup>7<sup>1</sup> state resulted in large differences in the  $A$  and  $C$  rotational constants from those determined in this work, as indicated in Table 4. While the 8<sup>1</sup>9<sup>1</sup> state distortional constants in Ref. [19] were well behaved in comparison to the corresponding ground state constants, two distortional constants for the 6<sup>1</sup>7<sup>1</sup> state were unreasonable large, with  $\Delta_K$  a factor of 20 and  $H_K$  a factor of 1000 larger than the ground state constants. As a result of the Hamiltonian model and the unphysical constants, the  $\nu_6 + \nu_7$  band origin is not as accurate as the uncertainty from the analysis would indicate. While the uncertainty in the band origin difference reported here could likewise be underestimated due

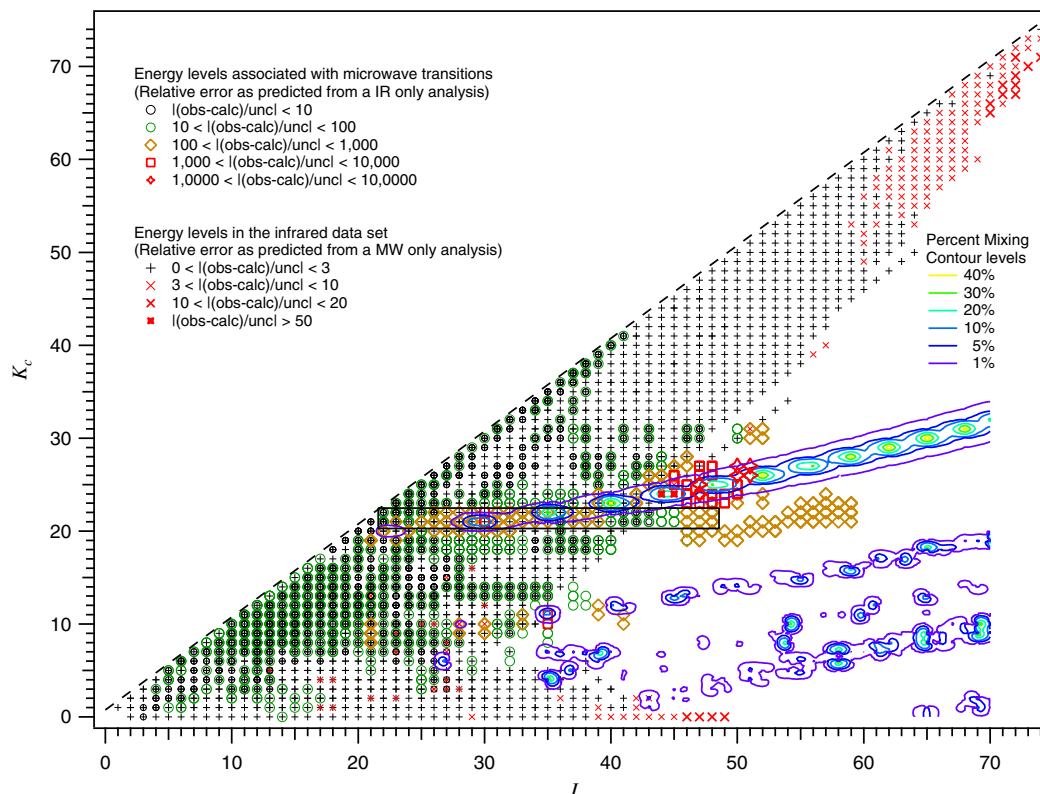


**Fig. 3.** Data distribution plots for the  $8^1_9^1$  state as a function of quantum numbers  $K_c$  and  $J$  showing the quantum states involved in the rotational transitions ('○', '◇', '□', and '×') or an infrared energy level ('+', '×', '×', and '×') from Ref. [19]. The sub symbols for each data set represent the relative error from the predictions based on an analysis of the other data set (i.e. microwave-only analysis predicting the infrared data or vice versa). A contour plot of the vibrational wavefunction mixing coefficients as a function of quantum number is overlaid. The contours are due to localized  $\Delta K_c = 2$  Fermi resonances and show the percent mixing of the wavefunctions. The larger rectangle spanning the  $J = 22-48$  and  $K_c = 21, 22$  shows the represented quantum numbers associated with the Q-branch transitions plotted in Fig. 5.

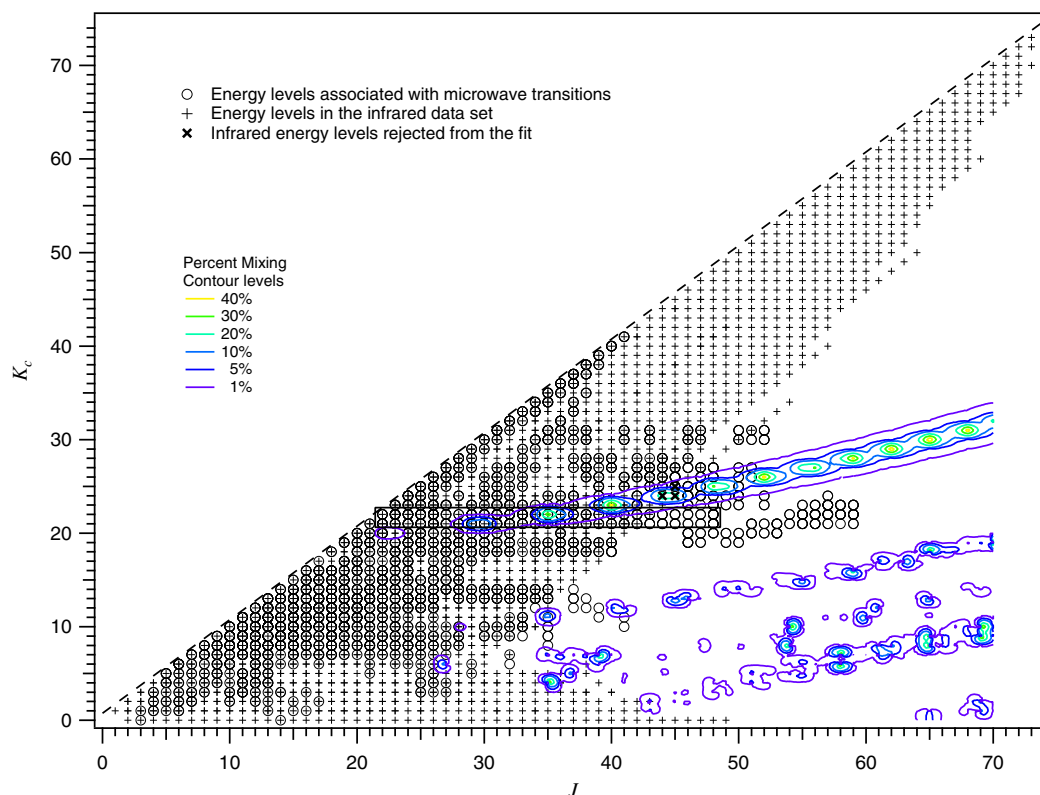


**Fig. 4.** Data distribution plots for the  $6^1_7^1$  state as a function of quantum numbers  $K_c$  and  $J$  showing the quantum states involved in the microwave rotational transitions ('○') or the one infrared energy level ('+') from Ref. [19]. A contour plot of the vibrational wavefunction mixing coefficients as a function of quantum number is overlaid. The contours are due to localized  $\Delta K_c = 2$  Fermi resonances and show the percent mixing of the wavefunctions.

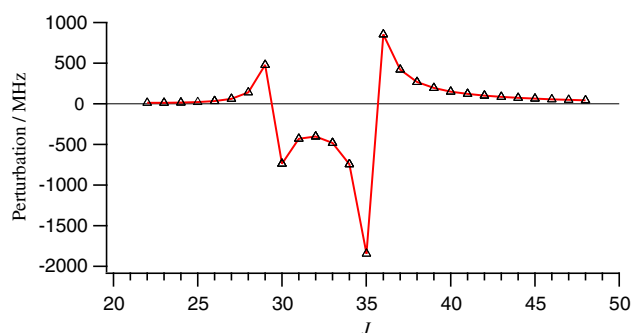


**Fig. 5.** Frequency difference plot for the  $8^1_9^1$  Q-branch ( $K_c = 21 \rightarrow 22$ ) showing the shift in the transition frequencies due to the localized Fermi resonance. This branch corresponds to the levels enclosed by the rectangle in Fig. 3 and was calculated by setting the Fermi interactions terms to zero in the final analysis and predicting the resulting spectrum. The triangles indicate measured transitions and the effect of two local resonances centered at ( $J = 29-30$ ,  $K_c = 21$ ) and ( $J = 35$ ,  $K_c = 22$ ) can be seen on transition frequencies.

**Table 3**

Torsional splitting<sup>a</sup> for vibrational states of HNO<sub>3</sub>.

Vibrational state	Splitting (MHz)
$\nu_9 = 1$	2.3
$\nu_9 = 2^b$	50.8
$\nu_5 = 1^b$	35.4
$\nu_7 = \nu_9 = 1$	12.4
$\nu_6 = \nu_9 = 1$	22.5
$\nu_7 = 2$	–
$\nu_8 = \nu_9 = 1$	3.3
$\nu_6 = \nu_7 = 1$	1.4
$\nu_9 = 3$	1759.6
$\nu_6 = 2^c$	0.8
$\nu_4 = 1^d$	4.0
$\nu_3 = 1^d$	3.9
$\nu_7 = \nu_8 = 1^{c,d}$	2.3

<sup>a</sup> Defined as the torsional parameter  $2E_\rho$ .

<sup>b</sup> Alternatively, 86.2 MHz for  $\nu_9 = 2$  and 0.0 MHz for  $\nu_5 = 1$ .

<sup>c</sup> Tentative vibrational state assignment.

<sup>d</sup> As estimated from the measured spectrum rather than a fit.

**Table 4**

Comparison of fitted and predicted rotational constants.<sup>a</sup>

Constant	Obs. <sup>b</sup>	Ref. [16] <sup>c</sup>	Ref. [33] <sup>d</sup>	Ref. [19] <sup>e</sup>	Ref. [18] <sup>e</sup>
$\nu_6 = \nu_7 = 1$					
$\Delta A_\nu$ (MHz)	–12.97	–13.14	–17.79	–91.57	[0.0] <sup>f</sup>
$\Delta B_\nu$ (MHz)	48.39	43.70	36.18	43.39	45.00
$\Delta C_\nu$ (MHz)	35.89	37.33	35.88	2.06	[0.0] <sup>f</sup>
$\nu_8 = \nu_9 = 1$					
$\Delta A_\nu$ (MHz)	17.78	25.01	25.32	17.77	17.77
$\Delta B_\nu$ (MHz)	153.77	179.15	189.47	153.88	153.69
$\Delta C_\nu$ (MHz)	5.70	5.23	4.39	5.69	5.69

<sup>a</sup> Changes in the rotational constants from the ground state are considered to be the vibration–rotation constants where  $\Delta A_\nu = \alpha_\nu^A = A_{gs} - A_\nu$ .

<sup>b</sup> Observed (Obs) values are based on the fitted rotational constants in Table 1 after transforming the rotational constants to the principal axis system from the internal axis system.

<sup>c</sup> Calculated based on the corresponding observed values for the ground and fundamental vibrational states in Ref. [16].

<sup>d</sup> DFT values are based on the vibrational–rotational coefficients from a density functional theory calculation at the B3LYP level with a 6-311(d,p) basis set.

<sup>e</sup> Infrared analysis by Perrin et al. [19] and Wang et al. [18].

<sup>f</sup> Fixed at the ground state value and not fitted.

to the choice of the Hamiltonian model and fitted data, the direct measurement and extensive sampling of each state's rotational manifold will greatly improve the accuracy of the fitted parameters.

In the infrared analysis of Perrin et al. [19], the previously reported rotational spectrum by Goyette et al. [12] was not included in the analysis due to a number ( $\sim 14$ ) of significant differences between the measured frequencies and those predicted by the infrared analysis that were much larger than the predicted uncertainties for each analysis. Of the previously reported 107 transitions, 64 are in the current analysis reported here and 43 have been reassigned or removed from the analysis due to interfering lines from other states. Of the reassigned transitions, a majority ( $\sim 20$ ) were in the asymmetric-top limit and are associated with both weaker lines and the absence of the triplet structure used to assist in the identification of the transition. Other transitions were incorrectly assigned due to a congested spectrum. When compared to the analysis reported here, 15 of the previously assigned transitions in Ref. [12] are off by 20 MHz or more and the rotational data set presented here supersedes the one previously reported in Ref. [12]. The infrared analysis in Ref. [19] does well at predicting the  $8^1_9^1$  microwave transitions in Ref. [12]. For instance, when comparing the microwave predictions based on the infrared analysis in Ref. [19] to those of the current analysis for the corrected microwave data set of Ref. [12], there is an rms deviation of 0.8 MHz for 105 of the 107 transitions with no more than  $\sim 3$  MHz maximum difference between the two sets of predictions. However, the infrared-only predictions for two microwave transitions that involved the  $22_3 20$  level are off by  $\pm 30$  MHz due to a local Fermi resonance (2.8% wavefunction mixing). For the infrared analysis, while fitting the 'effective' rotational constants and Fermi resonance for the  $6^1_7^1$  state was sufficient to fit the perturbations associated with the infrared energy levels, greater detail of the  $6^1_7^1$  energy levels and more accurate constants are needed to accurately predict all of the local resonances that are shown in Figs. 3 and 4 that result in large shifts in the transition frequencies shown in Fig. 5. To illustrate this, Fig. 3 shows the complementary nature of the two data sets where one set of symbols represents the infrared data set and the other set represents the microwave data set in the final combined analysis whose statistics are provided in Table 2. The symbols sets are coded by the relative error in how the infrared data set is predicted by a microwave-only analysis and vice versa. As would be expected, the relative errors for the predictions are largest in the regions that are considered extrapolations from the measured data set for each individual analysis. For instance, the microwave-only analysis predicts the infrared energy levels with higher relative errors of 10–20 occurring for  $J > 60$  and for  $J \sim K_a$  above  $J \approx 40$  that are regions that fall outside of the levels measured in the microwave data set. The infrared-only analysis has extremely large relative errors ( $>100$  and over 1000 in some cases) along the  $\Delta K_a = \pm 2$  Fermi resonance regions and in the  $J \approx 45-60$ ,  $K_c \approx 19-24$  region that lies outside of the infrared data set. In this latter case, such large discrepancies are due the lack of  $6^1_7^1$  state data, Hamiltonian model and unphysical constants that resulted from the fit, as discussed above.

#### 4. Summary

The rotational spectrum of the  $8^1_9^1$  and  $6^1_7^1$  vibrational states of nitric acid (HNO<sub>3</sub>) has been analyzed in the range between 78 and 519 GHz. Over 900 transition frequencies in the  $8^1_9^1$  state and over 600 in the  $6^1_7^1$  state have been fit to experimental accuracy, along with the infrared energy levels in Ref. [19], to a Hamiltonian model that accurately accounts for the torsional splitting in each state and the localized  $\Delta K_a = \pm 2$  Fermi resonances. This model provides a description of the ro-vibrational energy level structure, determined the band origin difference between the two vibrational states to be  $17.733184(17)$  cm<sup>–1</sup>, and will provide an accurate simulation of the 8.3  $\mu$ m region. We have now published extensive

rotational analyses of all states up to and including the  $6^{171}$  state at  $1223\text{ cm}^{-1}$  that will provide a framework for infrared simulations, a better understanding the torsional splitting and ro-vibrational interactions, and permit further investigations into the cluster of vibrational modes in the  $\sim 1300\text{--}1500\text{ cm}^{-1}$  region that includes  $3\nu_9$ ,  $\nu_3$ ,  $\nu_4$ ,  $\nu_7 + \nu_8$ ,  $\nu_5 + \nu_9$ ,  $\nu_6 + \nu_8$ ,  $\nu_5 + \nu_7$ , and  $\nu_7 + 2\nu_9$ .

## Acknowledgments

This material is based upon work supported by NASA. The authors are also grateful to Dr. A. Perrin for the communication of the energy levels derived from high-resolution infrared measurements that were used in this work.

## Appendix A. Supplementary data

Supplementary data for this article are available on ScienceDirect ([www.sciencedirect.com](http://www.sciencedirect.com)) and as part of the Ohio State University Molecular Spectroscopy Archives ([http://msa.lib.ohio-state.edu/jmsa\\_hp.htm](http://msa.lib.ohio-state.edu/jmsa_hp.htm)).

Supplementary data associated with this article can be found, in the online version, at [doi:10.1016/j.jms.2010.04.002](https://doi.org/10.1016/j.jms.2010.04.002).

## References

- [1] P.J. Popp, T.P. Marcy, R.S. Gao, L.A. Watts, D.W. Fahey, E.C. Richard, S.J. Oltmans, M.L. Santee, N.J. Livesey, L. Froidevaux, B. Sen, G.C. Toon, K.A. Walker, C.D. Boone, P.F. Bernath, *J. Geophys. Res. Atmos.* 114 (2009) D03305.
- [2] A. Laraia, R.R. Gamache, J.M. Hartmann, A. Perrin, L. Gomez, *J. Quant. Spectrosc. Radiat. Transfer* 110 (2009) 687–699.
- [3] G. Brizzi, E. Arnone, M. Carlotti, B.M. Dinelli, J.M. Flaud, E. Papandrea, A. Perrin, M. Ridolfi, *J. Geophys. Res. Atmos.* 114 (2009) D16301.
- [4] G. Brizzi, M. Carlotti, J.M. Flaud, A. Perrin, M. Ridolfi, *Geophys. Res. Lett.* 34 (2007) L03802.
- [5] L. Gomez, H. Tran, A. Perrin, R.R. Gamache, A. Laraia, J. Orphal, P. Chelin, C.E. Fellows, J.M. Hartmann, *J. Quant. Spectrosc. Radiat. Transfer* 110 (2009) 675–686.
- [6] D.T. Petkie, T.M. Goyette, P. Helminger, H.M. Pickett, F.C. De Lucia, *J. Mol. Spectrosc.* 208 (2001) 121–135.
- [7] A. Perrin, J. Orphal, J.M. Flaud, S. Klee, G. Mellau, H. Mader, D. Walbrodt, M. Winnewisser, *J. Mol. Spectrosc.* 228 (2004) 375–391.
- [8] D.T. Petkie, P. Helminger, B.P. Winnewisser, M. Winnewisser, R.A.H. Butler, K.W. Jucks, F.C. De Lucia, *J. Quant. Spectrosc. Radiat. Transfer* 92 (2005) 129–141.
- [9] J.M. Flaud, G. Brizzi, M. Carlotti, A. Perrin, M. Ridolfi, *Atmos. Chem. Phys.* 6 (2006) 5037–5048.
- [10] A. Goldman, C.P. Rinsland, A. Perrin, J.-M. Flaud, *J. Quant. Spectrosc. Radiat. Transfer* 60 (1998) 851–861.
- [11] A. Maki, *J. Mol. Spectrosc.* 136 (1989) 105–108.
- [12] T.M. Goyette, F.C. De Lucia, *J. Mol. Spectrosc.* 139 (1990) 241–243.
- [13] L.H. Coudert, A. Perrin, *J. Mol. Spectrosc.* 172 (1995) 352–368.
- [14] C.D. Paulse, L.H. Coudert, T.M. Goyette, R.L. Crownover, P. Helminger, F.C. De Lucia, *J. Mol. Spectrosc.* 177 (1996) 9–18.
- [15] D.T. Petkie, P. Helminger, M. Behnke, I.R. Medvedev, F.C. De Lucia, *J. Mol. Spectrosc.* 233 (2005) 189–196.
- [16] D.T. Petkie, P. Helminger, R.A.H. Butler, S. Albert, F.C. De Lucia, *J. Mol. Spectrosc.* 218 (2003) 127–130.
- [17] B.J. Drouin, C.E. Miller, J.L. Fry, D.T. Petkie, P. Helminger, I.R. Medvedev, *J. Mol. Spectrosc.* 236 (2006) 29–34.
- [18] W.F. Wang, P.P. Ong, T.L. Tan, E.C. Looi, H.H. Teo, *J. Mol. Spectrosc.* 183 (1997) 407–413.
- [19] A. Perrin, J.-M. Flaud, F. Keller, A. Goldman, R.D. Blatherwick, F.J. Murcray, C.P. Rinsland, *J. Mol. Spectrosc.* 194 (1999) 113–123.
- [20] C. Chackerian, S.W. Sharpe, T.A. Blake, *J. Quant. Spectrosc. Radiat. Transfer* 82 (2003) 429–441.
- [21] D.T. Petkie, T.M. Goyette, R.P.A. Bettens, S.P. Belov, S. Albert, P. Helminger, F.C. De Lucia, *Rev. Sci. Instrum.* 68 (1997) 1675–1683.
- [22] S. Albert, D.T. Petkie, R.P.A. Bettens, S.P. Belov, F.C. De Lucia, *Anal. Chem.* 70 (1998) 719A–727A.
- [23] I. Medvedev, M. Winnewisser, F.C. De Lucia, E. Herbst, E. Bialkowska-Jaworska, L. Pyszczolkowski, Z. Kisiel, *J. Mol. Spectrosc.* 228 (2004) 314–328.
- [24] A.P. Cox, J.M. Riveros, *J. Chem. Phys.* 42 (1965) 3106–3112.
- [25] R.L. Crownover, R.A. Booker, F.C. De Lucia, P. Helminger, *J. Quant. Spectrosc. Radiat. Transfer* 40 (1988) 39–46.
- [26] H.M. Pickett, SPFIT/SPCAT Package. Available from: <http://spec.jpl.nasa.gov/>.
- [27] H.M. Pickett, *J. Mol. Spectrosc.* 148 (1991) 371–377.
- [28] H.M. Pickett, R.L. Poynter, E.A. Cohen, M.L. Delitsky, J.C. Pearson, H.S.P. Muller, *J. Quant. Spectrosc. Radiat. Transfer* 60 (1998) 883–890.
- [29] A. Perrin, Private Communication.
- [30] A. Perrin, J.M. Flaud, C. Camy-Peyret, B.P. Winnewisser, S. Klee, A. Goldman, F.J. Murcray, R.D. Blatherwick, F.S. Bonomo, D.G. Muircray, C.P. Rinsland, *J. Mol. Spectrosc.* 166 (1994) 224–243.
- [31] Z. Kisiel, E.B. Jaworska, R.A.H. Butler, D.T. Petkie, P. Helminger, I.R. Medvedev, F.C. De Lucia, *J. Mol. Spectrosc.* 254 (2009) 78–86.
- [32] D.T. Petkie, R.A.H. Butler, P. Helminger, F.C. De Lucia, *J. Mol. Struct.* 695–696 (2004) 287–293.
- [33] C. Gutle, J. Demaison, H.D. Rudolph, *J. Mol. Spectrosc.* 254 (2009) 99–107.